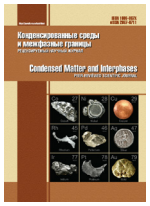

ISSN 1606-867X (Print)
ISSN 2687-0711 (Online)
Condensed Matter and Interphases
Kondensirovannye Sredy i Mezhfaznye Granitsy
https://journals.vsu.ru/kcmf/

Original articles

Research article
https://doi.org/10.17308/kcmf.2023.25/10973

Phase equilibria in the Cu_2SnSe_3–Sb_2Se_3–Se system

E. N. Ismayilova✉, L. F. Mashadiyeva, I. B. Bakhtiyarly, M. B. Babanly

Institute of Catalysis and Inorganic Chemistry n.a. M. Nagiyev of the Azerbaijan National Academy of Sciences, 113 H. Javid av., Baku Az1143, Azerbaijan

Abstract

Complex copper-tin and copper-antimony chalcogenides are of great interest for the development of new environmentally friendly and inexpensive thermoelectric materials. Recently, these compounds have been drawing more interest due to the possibility of increasing their thermoelectric performance with various cationic and anionic substitutions. In this article, we continued the study of multi-component systems based on the copper chalcogenides and presented the results of the study of phase equilibria in the Cu_2SnSe_3–Sb_2Se_3–Se system. The study was conducted using differential thermal analysis and powder X-ray diffraction.

Based on the experimental data, a projection of the liquidus surface and three polythermal cross sections of the phase diagram were plotted. We determined the regions of primary crystallisation of the phases and the nature and temperatures of non-variant and monovariant equilibria.

It was established that the liquidus surface consisted of two primary crystallisation regions based on Cu_2SnSe_3 and Sb_2Se_3 phases. The primary crystallisation region of elementary selenium was degenerate. A large immiscibility region of two liquid phases was found in the system.

Keywords: Phase diagram, Liquidus surface, Copper-antimony-tin selenides

Funding: The study was conducted as part of the scientific programme of the international laboratory "Promising materials for spintronics and quantum computing", created at the Institute of Catalysis and Inorganic Chemistry of Azerbaijan National Academy of Sciences (Azerbaijan) and the Donostia International Physics Center (Spain).

The work was partially supported by the Science Development Foundation under the President of the Republic of Azerbaijan – grant EİF-BGM-4-RFTF-1/2017-21/11/4-M-12.

For citation: Ismayilova E. N., Mashadiyeva L. F., Bakhtiyarly I. B., Babanly M. B. Phase equilibria in the Cu_2SnSe_3–Sb_2Se_3–Se system. *Condensed Matter and Interphases*. 2023;25(1): 47–54. https://doi.org/10.17308/kcmf.2023.25/10973

Для цитирования: Исмаилова Э. Н., Машадиева Л. Ф., Бахтиярлы И. Б., Бабанлы М. Б. Фазовые равновесия в системе Cu_2SnSe_3–Sb_2Se_3–Se. *Конденсированные среды и межфазные границы*. 2023;25(1): 47–54. https://doi.org/10.17308/kcmf.2023.25/10973

✉ Elnara N. Ismailova, e-mail: ismayilova818@mail.ru

1. Introduction

Copper-tin and copper-antimony chalcogenides form good basic phases for the development of materials with different functional properties [1–5]. Many of these phases are synthetic analogues of natural copper chalcogenide minerals, such as tetrahedrite, colusite, famatinite, etc., and they are of great interest for the development of new environmentally friendly and inexpensive thermoelectric materials. Studies showed that some of them demonstrated highly effective thermoelectric properties in the medium temperature range (600÷800 K), and their presence was primarily due to the specific features of the crystal structure [6-10]. Recently, these compounds have been garnering more interest due to the possibility of increasing their thermoelectric performance with various cationic and anionic substitutions [11–22]. Moreover, these substitutions can be both homovalent and heterovalent. For instance, in [16-22] it was shown that Sn-containing famatinites $Cu_3Sb_{1-x}Sn_xS_4$ and tetrahedrites $Cu_{12-x}Sn_xSb_4S_{13}$ could be obtained where heterovalent substitution of Sb^{5+} for Sn^{4+} resulted in the increased thermoelectric performance.

It is known that we need reliable data on the phase equilibria of the corresponding systems in order to determine the conditions for the directed synthesis of compounds and nonstoichiometric phases based on them, as well as to grow single crystals [23, 24]. In some previous works [25-28], we conducted similar comprehensive studies of complex systems based on copper and silver chalcogenides, in which we found new phases of variable compositions.

In [29, 30] we studied Cu_3SbSe_4–$SnSe_2(GeSe_2)$ systems in order to discover new phases of variable compositions based on the selenide analogue of the famatinite mineral. It was found that the solubility based on Cu_3SbSe_4 was up to 20 mol %. In the regions with lower content of Cu_3SbSe_4 phase equilibria had a complex nature. According to [29], it was associated with the stability of the Cu_2GeSe_3–Sb_2Se_3–Se concentration triangle, which led to a formation of four-phase regions in the Cu_2Se–$GeSe_2$–Sb_2Se_3–Se tetrahedron: Cu_3SbSe_4+Cu_2GeSe_3+Sb_2Se_3+Se и Cu_2GeSe_3+Sb_2Se_3+$GeSe_2$+Se. A similar situation is observed in the Cu_3SbSe_4-$SnSe_2$ system [30].

The goal of the present work was to determine the nature of phase equilibria in the Cu_2SnSe_3-Sb_2Se_3-Se concentration triangle, which play a decisive role in the formation of the complete picture of phase equilibria in the Cu_2Se-$SnSe_2$-Sb_2Se_3-Se subsystem. In previous works [31-35], other independent subsystems Cu_2Se-SnSe-Sb_2Se_3 and Cu_2Se-$SnSe_2$-Sb_2Se_3 of the Cu-Sn-Sb-Se quaternary system were studied, and a number of polythermal and isothermal sections as well as a projection of the liquidus surface were plotted.

1.1. Starting compounds

The starting compound Sb_2Se_3 of the studied system melts congruently at 863 K and forms a degenerate eutectic with selenium at 493 K [36]. Antimony selenide Sb_2Se_3 crystallises in the orthorhombic lattice (space group *Pnma*): a = 11.7938(9) Å, b = 3.9858(6) Å, and c = 11.6478(7) Å, z = 4 [37].

Cu_2SnSe_3 compound melts congruently at 968 K has a polymorphic transition at 948 K [38, 39]. The high-temperature modification crystallises in a cubic structure with the parameter of the lattice a = 5.6877 Å [38, 40], while the low-temperature modification crystallises in the monoclinic structure (space group *Cc*) with the parameters of the unit cell a = 6.9670±3 Å, b = 12.0493±7 Å, c = 6.9453±3 Å, β = 109.19(1)°; z = 4 [41, 42]. This compound forms a state diagram of the eutectic type with the Sb_2Se_3 compound with insignificant mutual solubility (not more than 2%) of the initial components. The coordinates of the eutectic point were 72 mol % Sb_2Se_3 and 769 K [31]. The Cu_2SnSe_3–6Se boundary system forms a *T-x* diagram with a degenerate eutectic equilibrium at 493 K and a wide region of immiscibility (37–95 mol % Se) at 910 K [39].

2. Experimental

2.1. Synthesis

Simple high-purity substances by Evochem Advanced Materials GMBH (Germany) were used for the experiments: copper granules (Cu-00029; 99.9999%), antimony granules (Sb-00002; 99.999%), tin granules (Sn-00005; 99.999%), and selenium granules (Se-00002; 99.999%). Starting compounds Cu_2SnSe_3 and Sb_2Se_3 were synthesised by melting simple substances in stoichiometric proportions in vacuumed to ~10^{-2} Pa and

sealed quartz ampoules at temperatures 50° higher than the melting temperatures of the synthesised compounds. The Cu_2SnSe_3 compound was synthesised in a two-zone sloping furnace. The temperature of the lower "hot" zone was 1050 K, and the temperature of the upper "cold" zone was 900 K, which is slightly lower than the boiling point of selenium (958 K [43]). After the overall reaction of selenium, the ampoule with a sample was placed completely into the hot zone of the furnace and kept at this temperature for 3–4 hours. After the synthesis, the ampoule with Cu_2SnSe_3 was cooled to room temperature in the switched-off furnace.

The individuality of the synthesised compounds Cu_2SnSe_3 and Sb_2Se_3 was controlled using differential thermal analysis (DTA) and powder X-ray diffraction (XRD). The obtained melting point values and parameters of crystal lattices of all synthesised compounds within the measure of inaccuracy (±3 K and ±0.0003 Å) were similar to the above mentioned literature data.

Approximately 30 alloys were prepared in accordance with the studied sections together with additional alloys in order to conduct the experiments through melting the initial compounds in vacuum. The DTA data for cast non-homogenised alloys showed that their crystallisation from melts was completed at ~490 K. Therefore, the cast alloys obtained by quick cooling of melts were first annealed at 650 K for 200 hours, and then at 450 K for 300 hours. This was done in order to achieve the state as similar to the equilibrium as possible.

2.2. Research methods

DTA was conducted in the range of temperatures from room temperature to 1100 K with a heating rate of 10 K·min^{-1} on a 404 F1 PEGASUS SYSTEM differential scanning calorimeter (NETZSCH). The measurement results were processed using the NETZSCH Proteus Software. The temperature measurement accuracy was within ±2 K.

X-ray phase analysis was performed at room temperature on a D8 ADVANCE diffractometer (BRUKER) with Cu$K\alpha_1$ radiation. The XRD patterns were indexed using Topas V3.0 Software Bruker.

3. Results and discussion

XRD of the selected alloys showed that they consisted of a three-phase mixture Cu_2SnSe_3+Sb_2Se_3+Se. A powder diffraction pattern of the alloy of the 1/6Cu_2SnSe_3-1/5Sb_2Se_3-Se system with the 4:4:2 ratio of the initial components, respectively, is presented in Fig. 1 as an example. It can be seen that the diffraction pattern of the alloy consists of a set of reflection lines of Cu_2SnSe_3, Sb_2Se_3, and grey crystalline selenium.

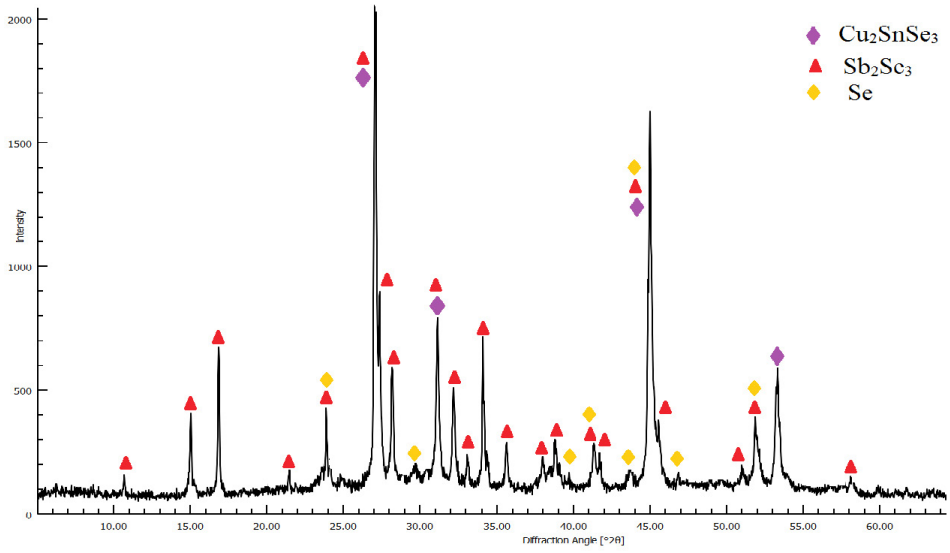

Fig. 1. Powder diffraction pattern of the alloy of the 1/6Cu_2SnSe_3–1/5Sb_2Se_3–Se system with the 4:4:2 ratio of the initial components, respectively

3.1. Liquidus surface

The liquidus surface of the Cu_2SnSe_3-Sb_2Se_3-Se system (Fig. 2) consists of two main and one degenerate sections. Region 1 corresponds to primary crystallisation of α_1 and α_2 phases based on two crystalline modifications of Cu_2SnSe_3, while region 2 corresponds to primary crystallisation of β-solid solutions based on Sb_2Se_3. The third region corresponds to elemental selenium and was degenerate in the corresponding angle of the concentration triangle.

A typical feature of the system is that the immiscibility region existing on the side quasi-binary section of Cu_2SnSe_3–Se (contour mm^1 at 910 K) suddenly penetrates inside the triangle forming a wide region ($mMKM^1m^1$) of immiscibility of two liquid phases (L_1+L_2). As Fig. 2 shows, this region crosses the curve coming out from the eutectic point (e_1) of the Cu_2SnSe_3–Sb_2Se_3 system and takes a part of the liquidus surface of β-phase (MKM^1). In the MM^1 interval the eutectic curve crosses the immiscibility region, and the eutectic equilibrium L ↔ α+β turns into a non-variant monotectic equilibrium L ↔ L_2+α+β.

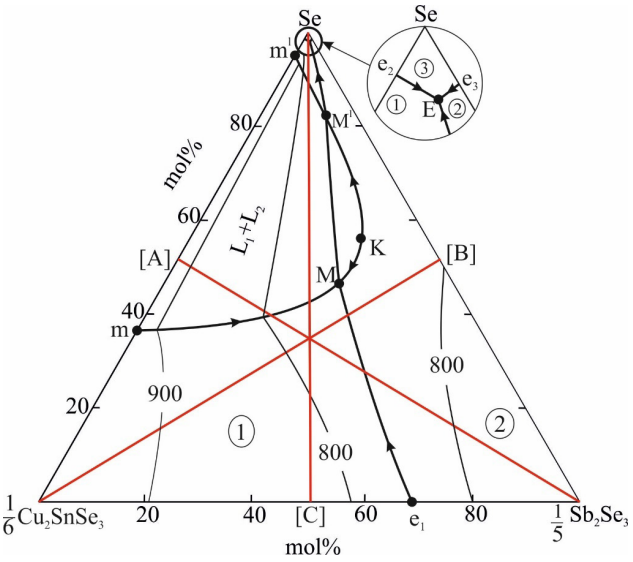

Fig. 2. Liquidus surface of the Cu_2SnSe_3–Sb_2Se_3–Se system. Primary crystallisation fields: *1* – α (solid solution based on Cu_2SnSe_3); *2* – β (solid solution based on Sb_2Se_3); *3* – Se. Red lines are the studied polythermal sections

All non-variant and monovariant phase equilibria observed in the system, including side systems, are presented in Table 1. Fig. 2 and Table 1 show that the conjugated curves mM и mM^1 limiting the immiscibility region reflect the process of crystallisation of α-phase while the conjugated curves MK and KM^1 reflect the monovariant crystallisation of β-phase upon monotectic reactions.

The process of crystallisation in the system completes with the formation of a triple eutectic mixture α_2+β+Se (E; 490 K). Eutectic points e_2 and e_3 on boundary quasi-binary systems as well as point E and eutectic curves e_2E и e_3E are degenerate. This part of the phase diagram is presented in Fig. 2 as an enlarged view (representative scale).

3.2. Polythermal sections

We will consider three polythermal sections of the phase diagram perpendicular to side systems in the context of Fig. 2 and Table 1 to obtain a better visual description of the crystallisation processes in the system, especially those

Table 1. Non-variant and monovariant phase equilibria in the Cu_2SnSe_3–Sb_2Se_3–Se system

Point or curve in fig. 2	Equilibrium	Composition, mol %		*T*, K
		$0{,}2Sb_2Se_3$	Se	
m(m^1)	$L_1 \leftrightarrow L_2+\alpha$	-	36(95)	910
e_1	$L \leftrightarrow \alpha+\beta$	68	-	769
e_2	$L \leftrightarrow \alpha+Se$	-	>99	493
e_3	$L \leftrightarrow \beta+Se$	<1	>99	491
M(M^1)	$L_1 \leftrightarrow L_2+\alpha+\beta$	35(13)	45(82)	730
E	$L \leftrightarrow \alpha+\beta+Se$	<1	>98	490
e_1M	$L_1 \leftrightarrow \alpha+\beta$			769-730
M^1E	$L_2 \leftrightarrow \alpha+\beta$			730-490
e_2E	$L \leftrightarrow \alpha+Se$			493-490
e_3E	$L \leftrightarrow \alpha+Se$			491-490
$mM(m^1M^1)$	$L_1 \leftrightarrow L_2+\alpha$			910-730
$KM(KM^1)$	$L_1 \leftrightarrow L_2+\beta$			750-730

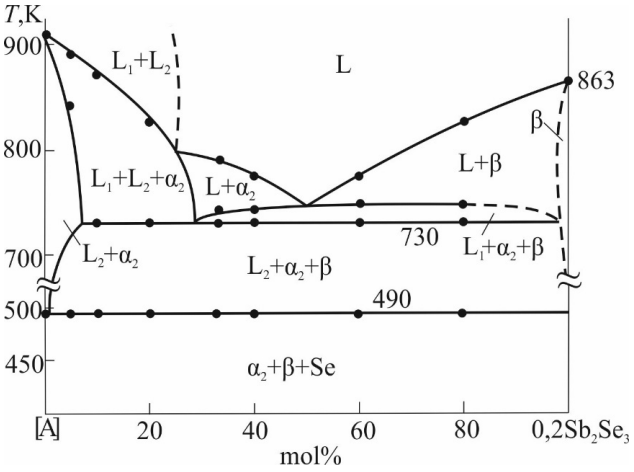

Fig. 3. Phase diagram of the [A]-$0.2Sb_2Se_3$ system. [A] – alloy of the Cu_2SnSe_3–6Se system with the composition 1:1

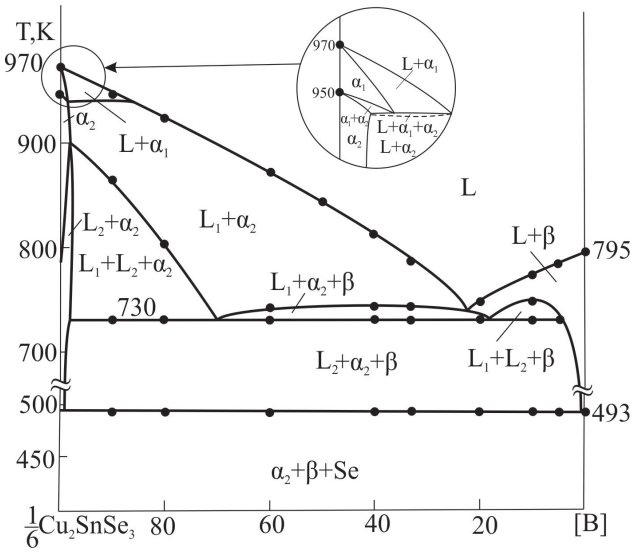

Fig. 4. Phase diagram of the [B]–$1.6Cu_2SnSe_3$ system. [B] – alloy of the $1/5Sb_2Se_3$–Se side system with the composition 1:1

below the liquidus surface and the region of immiscibility.

Section [A]–0,2 Sb_2Se_3 (where [A] is an alloy of the Cu_2SnSe_3-6Se side system corresponding to the composition 1:1). This section crosses the region of immiscibility and the liquidus surface of α and β phases (Fig. 3). The two-phase region $L_1 + L_2$ is limited by the region of L-liquid solution with a dotted line. The curves below the regions L_1+L_2, L+α and L+β reflect the monovariant mM (m^1M^1) monotectic (0–28 mol % $0.2Sb_2Se_3$) and eutectic e_1M (28–99 mol % $0.2Sb_2Se_3$) equilibria. As a result of these processes, three-phase regions $L_1+L_2+\alpha$ и $L_1+\alpha+\beta$ are formed in Fig. 3.

At 730 K, the non-variant monotectic equilibrium M is implemented in the system, and this reaction is completed with the formation of a three-phase region $L_2+\alpha+\beta$. Finally, the horizontal line corresponding to 490 K represents the crystallisation of the ternary eutectic (E).

Section $1/6Cu_2SnSe_3$–[B] (Fig. 4) (where [B] is an alloy of the $1/5Sb_2Se_3$-Se side system corresponding to the composition 1:1). This section does not pass through the immiscibility region. The liquidus consists of 3 curves of primary crystallisation of two modifications of Cu_2SnSe_3 (α_1 and α_2 phases) and β-phase based on Sb_2Se_3. The formation of solid solutions based on two modifications Cu_2SnSe_3 is accompanied by the lowered temperature of the polymorphic transition of this compound and establishment of a monovariant metatectic reaction $\alpha_1 \leftrightarrow L+\alpha_2$.

The corresponding three-phase region is located in a very narrow range of temperatures and is separated by a dotted line. This part of the phase diagram is presented in Fig. 2 as an enlarged view (representative scale). The comparison of this diagram with Fig. 3 shows that the curves below liquidus also reflect monotectic equilibria. In the range of compositions 0–30; 30–80 and 80–95 mol % [B] monovariant reactions process according to mM, e_1M, and KM, which leads to the formation of regions ($L_1+L_2+\alpha$), ($L_1+\alpha+\beta$), and ($L_1+L_2+\beta$) in Fig. 4. With lower temperatures, crystallisation continues in accordance with non-variant monotectic reaction M (730 K) and ends with a non-variant eutectic process E (490 K).

Section [C]–Se (Fig. 5) (where [C] is an alloy of the $1/6Cu_2SnSe_3$–$1/5Sb_2Se_3$ side system corresponding to the composition 1:1). This section is almost completely located in the region of primary crystallisation of the α-phase, and in the concentration range of 40–90 at. % Se (el.) it passes through the region of immiscibility of two liquids. In the range of compositions of 0-40 at. % Se (el.) α-phase crystallises from the liquid phase L_1 based on selenides, while in the range of >90 at. % Se (el.) crystallises from the liquid phase L_2 based on selenium. Monovariant and non-variant processes occurring below liquidus can be easily determined in the context of Fig. 2.

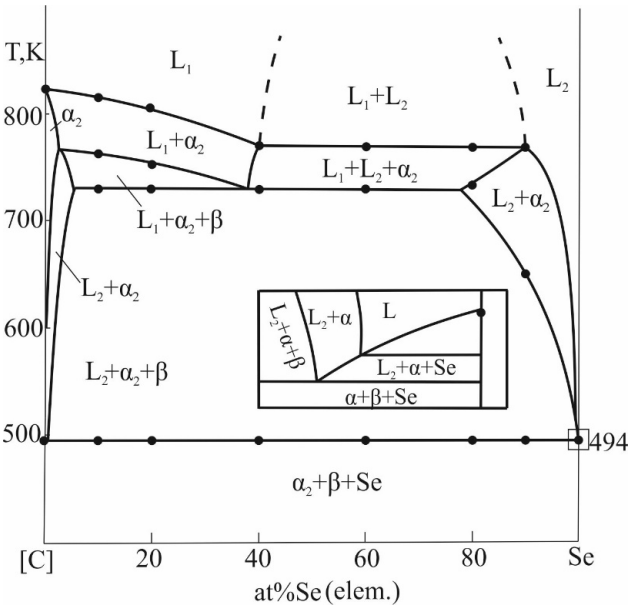

Fig. 5. Phase diagram of the [C]–Se system. [C] – alloy of the $1/6Cu_2SnSe_3$–$1/5Sb_2Se_3$ side system corresponding to the composition 1:1

4. Conclusions

Thus we obtained the complete picture of phase equilibria in the Cu_2SnSe_3-Sb_2Se_3-Se system. It was established that it is a quasi-ternary plane corresponding to the quaternary system. The liquidus surface consisted of three primary crystallisation fields α and β of solid solutions based on Cu_2SnSe_3 и Sb_2Se_3, respectively, as well as of elemental selenium. The region of crystallisation of elemental selenium was degenerate in the corresponding angle of the concentration triangle. A formation of a wide region of immiscibility permeating from the Cu_2SnSe_3–Se side system inside the Cu_2SnSe_3–Sb_2Se_3-Se concentration triangle was a typical feature of the studied system.

Author contributions

E. N. Ismayilova – research concept, conducting research, synthesis of compounds, article writing, discussion of results. L. F. Mashadiyeva – analysis of scientific literature, discussion of results. I. B. Bakhtiyarly – discussion of results. M. B. Babanly – research concept, final conclusions.

Conflict of interests

The authors declare that they have no known competing financial interests or personal relationships that could have influenced the work reported in this paper.

Referenses

1. Alonso-Vante N. *Chalcogenide materials for energy conversion. Pathways to oxygen and hydrogen reactions*. Springer Cham; 2018. 226 p. https://doi.org/10.1007/978-3-319-89612-0

2. *Applications of Chalcogenides: S, Se, and Te*. Ahluwalia G. K. (ed.). Cham. Springer, 2016. 461 p. https://doi.org/10.1007/978-3-319-41190-3

3. *Chalcogenides: Advances in research and applications*. Nova P. W. (ed.). 2018. 111 p.

4. Peccerillo E., Durose K. Copper–antimony and copper–bismuth chalcogenides—Research opportunities and review for solar photovoltaics. *MRS Energy & Sustainability*. 2018;5(1): 1–59. https://doi.org/10.1557/mre.2018.10

5. Sanghoon X. L., Tengfei L. J., Zhang L. Y-H. *Chalcogenide. From 3D to 2D and beyond*. Elsevier; 2019. 398 p.

6. Suekun K., Takabatake T. Research update: Cu–S based synthetic minerals as efficient thermoelectric materials at medium temperatures. *APL Materials*. 2016;4: 104503. https://doi.org/10.1063/1.4955398

7. Chetty R., Bali A., Mallik R. C. Tetrahedrites as thermoelectric materials: an overview. *Journal of Materials Chemistry C*. 2015;3(48): 12364–12378. https://doi.org/10.1039/c5tc02537k

8. Kim F. S., Suekuni K., Nishiate H., Ohta M., Tanaka H. I., Takabatake T. Tuning the charge carrier density in the thermoelectric colusite. *Journal of Applied Physics*. 2016;119(17): 175105. https://doi.org/10.1063/1.4948475

9. Powell A. V. Recent developments in Earth-abundant copper-sulfide thermoelectric materials. *Journal of Applied Physics,* 2019;126(10): 100901. https://doi.org/10.1063/1.5119345

10. Mikuła A., Mars K., Nieroda P., Rutkowski P. Copper chalcogenide-copper tetrahedrite composites – a new concept for stable thermoelectric materials dased on the chalcogenide system. *Materials*. 2021;14(10): 2635. https://doi.org/10.3390/ma14102635

11. Sobolev A. V., Presniakov I. A., Nasonova D. I., Verchenko V. Yu., Shevelkov, A. V. Thermally-activated electron exchange in $Cu_{12-x}Fe_xSb_4S_{13}$ (x = 1.3, 1.5) tetrahedrites: a Mössbauer study. *The Journal of Physical Chemistry C*. 2017;121(8): 4548–4557. https://doi.org/10.1021/acs.jpcc.6b12779

12. Sun F.-H., Dong J., Dey S., … Li J.-F. Enhanced thermoelectric performance of $Cu_{12}Sb_4S_{13}$–δ tetrahedrite via nickel doping. *Science China Materials*. 2018;61(9): 1209–1217. https://doi.org/10.1007/s40843-018-9241-x

13. Deng S., Jiang X., … Tang X. The reduction of

thermal conductivity in Cd and Sn co-doped Cu_3SbSe_4-based composites with a secondary-phase CdSe. *Journal of Materials Science*, 2020;56(7): 4727–4740. https://doi.org/10.1007/s10853-020-05586-3

14. Zhao D., Wu D., Bo L. Enhanced thermoelectric properties of Cu_3SbSe_4 compounds via gallium doping. *Energies*. 2017;10(10): 1524. https://doi.org/10.3390/en10101524

15. Liu G., Li J., Chen K., … Li, L. Direct fabrication of highly-dense $Cu_2ZnSnSe_4$ bulk materials by combustion synthesis for enhanced thermoelectric properties. *Materials & Design*. 2016;93: 238–246. https://doi.org/10.1016/j.matdes.2015.12.172

16. Liu M., Qin X., Liu C. Substitution site selection and thermoelectric performance-enhancing mechanism of $Cu_{12}Sb_4S_{13}$ doped with Pb/Ge/Sn. *Physica Status Solidi B*. 2022;259: 2100275–2100278. https://doi.org/10.1002/pssb.202100275

17. Chen K., Di Paola C., Laricchia S., … Bonini N. Structural and electronic evolution in the Cu_3SbS_4–Cu_3SnS_4 solid solution. *Journal of Materials Chemistry C*. 2020;8(33): 11508–11516. https://doi.org/10.1039/d0tc01804j

18. Nasonova D. I., Sobolev A. V., Presniakov I. A., Andreeva K. D., Shevelkov A. V. Position and oxidation state of tin in Sn-bearing tetrahedrites $Cu_{12-x}Sn_xSb_4S_{13}$. *Journal of Alloys and Compounds*, 2019;778: 774–778. https://doi.org/10.1016/j.jallcom.2018.11.168

19. Wei T.-R., Wang H., Gibbs Z. M., … Li J.-F. Thermoelectric properties of Sn-doped *p*-type Cu_3SbSe_4: a compound with large effective mass and small band gap. *Journal* of *Materials Chemistri A*. 2014;2(33): 13527–13533. https://doi.org/10.1039/c4ta01957a

20. Tippireddy S., Prem Kumar D. S., Karati A., … Mallik R. C. Effect of Sn substitution on the thermoelectric properties of synthetic tetrahedrite. *ACS Applied Materials and Interfaces*. 2019;116(24): 21686–21696. https://doi.org/10.1021/acsami.9b02956

21. Chen K., Di Paola C., Du B., … Reece, M. Enhanced thermoelectric performance of Sn-doped Cu_3SbS_4. *Journal of Materials Chemistry C*. 2018;6(31): 8546–8552. https://doi.org/10.1039/c8tc02481b

22. Pi J.-H., Lee G.-E., Kim I.-H. Effects of Sn-doping on the thermoelectric properties of famatinite. *Journal of Electronic Materials*. 2019;49(5): 2755 – 2761. https://doi.org/10.1007/s11664-019-07710-9

23. Babanly M. B., Chulkov E. V., Aliev Z. S., Shevel'kov A. V., Amiraslanov I. R. Phase diagrams in materials science of topological insulators based on metal chalcogenides. *Russian Journal of Inorganic Chemistry*. 2017;62(13): 1703–1729. https://doi.org/10.1134/s0036023617130034

24. Imamaliyeva S. Z., Babanly D. M., Tagiev D. B., Babanly M. B. Physicochemical aspects of development of multicomponent chalcogenide phases having the Tl_5Te_3 structure: A Review. *Russian Journal of Inorganic Chemistry*. 2018;13: 1703–1027. https://doi.org/10.1134/s0036023618130041

25. Alverdiyev I. J., Aliev Z. S., Bagheri S. M., Mashadiyeva L. F., Yusibov Y. A., Babanly M. B. Study of the $2Cu_2S+GeSe_2 \leftrightarrow Cu_2Se+GeS_2$ reciprocal system and thermodynamic properties of the $Cu_8GeS_{6-x}Se_x$ solid solutions. *Journal of Alloys and Compounds*. 2017;691: 255–262. doi: https://doi.org/10.1016/j.jallcom.2016.08.251

26. Mashadiyeva L. F., Kevser J. O., Aliev I. I., Yusibov Y. A., Taghiyev D. B., Aliev Z. S., Babanlı M. B. The Ag_2Te-SnTe-Bi_2Te_3 system and thermodynamic properties of the $(2SnTe)_{1-X}(AgBiTe_2)_X$ solid solutions series. *Journal of Alloys and Compounds*. 2017;724: 641–648. https://doi.org/10.1016/j.jallcom.2017.06.338

27. Mashadiyeva L. F., Kevser J. O., Aliev I. I., Yusibov Y. A., Taghiyev D. B., Aliev Z. S., Babanlı M. B. Phase equilibria in the Ag_2Te-SnTe-Sb_2Te_3 system and thermodynamic properties of the $(2SnTe)_{12x}(AgSbTe_2)_x$ solid solution. *Phase Equilibria and Diffusion*. 2017;38(5): 603–614. https://doi.org/10.1007/s11669-017-0583-2

28. Bagheri S. M., Alverdiyev I. J., Aliev Z. S., Yusibov Y. A., Babanly M. B. Phase relationships in the $1.5GeS_2+Cu_2GeSe_3 \leftrightarrow 1.5GeSe_2+Cu_2GeS_3$ reciprocal system. *Journal of Alloys and Compounds*. 2015;625: 131–137. https://doi.org/10.1016/j.jallcom.2014.11.118

29. Ismayilova E. N., Baladzhayeva A. N., Mashadiyeva L. F. Phase equilibria along the Cu_3SbSe_4-$GeSe_2$ section of The Cu-Ge-Sb-Se. *New Materials, Compounds and Applications*. 2021;5(1): 52–58. Режим доступа: http://jomardpublishing.com/UploadFiles/Files/journals/NMCA/V5N1/Ismayilova_et_al.pdf

30. Ismayilova E. N. X-ray study of phase equilibria of the Cu_3SbSe_4-$SnSe_2$. *News of Azerbaijan Higher Technical Educational Institutions*. 2021;23(5): 21–25. Режим доступа: https://zenodo.org/record/7621101

31. Ostapyuk T. A., Yermiychuk I. M., Zmiy O. F., Olekseyuk I. D. Phase equilibria in the quasiternary system Cu_2Se–$SnSe_2$–Sb_2Se_3. *Chemistry of Metals and Alloys*. 2009;2: 164–169. https://doi.org/10.30970/cma2.0100

32. Ismayilova E. N., Mashadieva L. F. Фазовые равновесия в системе Cu_2Se-SnSe-Sb_2Se_3 по разрезу SnSe-Cu_3SbSe_3. Конденсированные среды и межфазные границы. 2018;20(2): 218–221. https://doi.org/10.17308/kcmf.2018.20/553

33. Ismailova E. N., Mashadieva L. F., Bakhtiyarly I. B., Babanly M. B. Phase equilibria in the Cu_2Se–SnSe–$CuSbSe_2$ system. *Russian Journal of Inorganic Chemistry*. 2019;64(6): 801–809. https://doi.org/10.1134/S0036023619060093

34. Ismailova E. N, Bakhtiyarly I. B, Babanly M. B. Refinement of the phase diagram of the SnSe-Sb_2Se_3 system. *Chemical Problems*. 2020;18(2): 250-256.

https://doi.org/10.32737/2221-8688-2020-2-250-256

35. Ismayilova E. N., Mashadiyeva L. F., Bakhtiyarly I. B., Babanly M. B. Phase equilibria in the Cu_2Se-SnSe-Sb_2Se_3 system. *Azerbaijan Chemical Journal*. 2022;1: 73–82. https://doi.org/10.32737/0005-2531-2022-1-73-82

36. *Binary alloy phase diagrams - second edition*. T. B. Massalski, H. Okamoto, P. R. Subramanian, L. Kacprzak (eds.). Ohio, USA: ASM International, Materials Park; 1990. 3589 p.

37. Voutsas G. P., Papazoglou A. G., Rentzeperis P. J., Siapkas D. The crystal structure of antimony selenide, Sb_2Se_3. *Zeitschrift für Kristallographie - Crystalline Materials*. 1985;171: 261–268. https://doi.org/10.1524/zkri.1985.171.14.261

38. Parasyuk O. V., Olekseyuk I. D., Marchuk O. V. The Cu_2Se–HgSe–$SnSe_2$ system. *Journal of Alloys and Compounds*. 1999; 287(1-2): 197–205. https://doi.org/10.1016/S0925-8388(99)00047-X

39. Babanly M. B., Yusibov Yu. A., Abishov V. T. *Three-component chalcogenides based on copper and silver**. Baku: BSU Publ.; 1993. 342 p. (In Russ.).

40. Sharma B.B., Ayyar R., Singh H. Stability of the Tetrahedral Phase in the $A^I_2B^{IV}C^{VI}_3$ Group of Compounds. *Physica Status Solidi A*. 1977;A40(2): 691–697. https://doi.org/10.1002/pssa.2210400237

41. Marcano G., Chalbaud L., Rincón C., Sánchez P. G. Crystal growth and structure of the semiconductor Cu_2SnSe_3. *Materials Letters*. 2002;53(3): 151–154. https://doi.org/10.1016/s0167-577x(01)00466-9

42. Delgado G. E., Mora A. J., Marcano G., Rincon C. Crystal structure refinement of the semiconducting compound Cu_2SnSe_3 from X-ray powder diffraction data. *Materials Research Bulletin*. 2003;38: 1949–1955. https://doi.org/10.1016/j.materresbull.2003.09.017

43. Emsley J. *The Elements*. Oxford University Press; 1998. 300 p.

** Translated by author of the article.*

Information about of authors

Elnara N. Ismailova, PhD student, Researcher, Institute of Catalysis and Inorganic Chemistry of the National Academy of Sciences of Azerbaijan (Baku, Azerbaijan).

https://orcid.org/0000-0002-1327-1753

ismayilova818@mail.ru

Leyla F. Mashadiyeva, PhD in Chemistry, Senior Researcher, Institute of Catalysis and Inorganic Chemistry of the National Academy of Sciences of Azerbaijan (Baku, Azerbaijan).

https://orcid.org/0000-0003-2357-6195

leylafm76@gmail.com

Ikhtiyar B. Bakhtiyarly, Dr. Sci. (Chem.), Professor, Head of laboratory, Institute of Catalysis and Inorganic Chemistry of the National Academy of Sciences of Azerbaijan (Baku, Azerbaijan).

https://orcid.org/0000-0002-7765-0672

ibbakhtiarli@mail.ru

Mahammad B. Babanly, Dr. Sci. (Chem.), Professor, Associate Member of the Azerbaijan National Academy of Sciences, Executive Director of the Institute of Catalysis and Inorganic Chemistry, Azerbaijan National Academy of Sciences (Baku, Azerbaijan).

https://orcid.org/0000-0001-5962-3710

babanlymb@gmail.com

Received 28.06.2022; approved after reviewing 05.10.2022; accepted for publication 15.11.2022; published online 25.03.2023.

Translated by Marina Strepetova

Edited and proofread by Simon Cox